BASIC SCIENCE

Nanomedicine: Nanotechnology, Biology, and Medicine
23 (2020) 102086

nanomedicine
Nanotechnology, Biology, and Medicine

nanomedjournal.com

Original Article

pH-triggered delivery of magnetic nanoparticles depends on tumor volume

Alexandra G. Pershina, PhD[a,b,*], Olga Ya. Brikunova, MSc[a,b], Alexander M. Demin, PhD[c], Oleg B. Shevelev, Specialist degree[d], Ivan A. Razumov, DrSci[d], Evgenii L. Zavjalov, PhD[d], Dina Malkeyeva, MSc[d], Elena Kiseleva, PhD[d], Nadezhda V. Krakhmal', PhD[a], Sergey V. Vtorushin, DrSci[a], Vasily L. Yarnykh, PhD[e,f], Vladimir V. Ivanov, PhD[a], Raisa I. Pleshko, DrSci[a], Victor P. Krasnov, DrSci[c], Ludmila M. Ogorodova, DrSci, MD[a]

[a]*Siberian State Medical University, Tomsk, Russia*
[b]*National Research Tomsk Polytechnic University, Tomsk, Russia*
[c]*Postovsky Institute of Organic Synthesis UB RAS, Yekaterinburg, Russia*
[d]*Institute of Cytology and Genetics SB RAS, Novosibirsk, Russia*
[e]*Department of Radiology, University of Washington, WA, USA*
[f]*Research Institute of Biology and Biophysics, National Research Tomsk State University, Tomsk, Russia*

Revised 4 July 2019

Abstract

Nowadays there is growing recognition of the fact that biological systems have a greater impact on nanoparticle target delivery in tumors than nanoparticle design. Here we investigate the targeted delivery of Fe_3O_4 magnetic nanoparticles conjugated with pH-low-insertion peptide (MNP-pHLIP) on orthotopically induced MDA-MB-231 human breast carcinoma xenografts of varying volumes as a model of cancer progression. Using *in vivo* magnetic resonance imaging and subsequent determination of iron content in tumor samples by inductively coupled plasma atomic emission spectroscopy we found that MNP-pHLIP accumulation depends on tumor volume. Transmission electron microscopy, histological analysis and immunohistochemical staining of tumor samples suggest that blood vessel distribution is the key factor in determining the success of the accumulation of nanoparticles in tumors.

Key words: pHLIP; Iron oxide magnetic nanoparticle; Tumor; MRI; Targeting

Despite the moderate advantages of antibody or peptide-conjugated nanoparticles in receptor-mediated tumor targeting, tumor heterogenicity and the binding-site barrier effect can hamper delivery success [1,2]. Specific physiological conditions formed in the tumors can serve as a viable alternative. Low extracellular pH is a common feature of many solid tumors [3]. Therefore, pH-low-insertion peptide (pHLIP) is applied for the delivery of labels and drugs to various types of tumors [4,5]. Recently, our research group has, for the first time, developed Fe_3O_4 magnetic nanoparticle (MNP) conjugated with pHLIP (MNP-pHLIP). Their ability to target LLC tumors in mice has previously been shown [6].

In spite of the growing number of published articles demonstrating the success of nanoparticle accumulation in tumors, a critical review revealed the limitations which hinder clinical application [7].

Since biological systems have a greater impact on targeted nanoparticle delivery than nanoparticle design [8], we need to closely evaluate the objective laws that regulate the behavior of nanoparticles *in vivo*. To this end, the orthotopic tumor xenograft model mimics tumor growth within the most relevant tissue environment and has some advantages compared to the ectopic model [9].

Here we investigate the pH-triggered delivery of Fe_3O_4 MNPs conjugated with pHLIP (MNP-pHLIP) on MDA-MB-231 human breast cancer xenografts. In the experiments tumors of varying volumes were induced orthotopically. Tumors of varying volumes have been used as a model of cancer progression by analogy with Sykes's research [8]. In order to better model clinical conditions, tumors in our study were relatively slow-growing and did not exceed 3.5% of total mouse body weight.

Authors list:
All authors declare no potential competing interests.
Funding: This work was supported by the Russian Foundation for Basic Research [grant number: 18-015-00319_a].
*Corresponding author at: 634050, Tomsk, Russia.
E-mail address: allysyz@mail.ru (A.G. Pershina).

https://doi.org/10.1016/j.nano.2019.102086
1549-9634/

Please cite this article as: Pershina AG, et al, pH-triggered delivery of magnetic nanoparticles depends on tumor volume. *Nanomedicine: NBM* 2020;23:102086, https://doi.org/10.1016/j.nano.2019.102086

Methods

Initial Fe_3O_4 MNPs were synthesized by co-precipitation method [10], modified with 3-aminopropylsilane (APS) [11] and conjugated with pHLIP (Scheme S1) according to protocols reported in [6]. The immobilization of pHLIP on the MNP-APS surface through 6-maleimidohexanoic acid *N*-hydroxysuccinimide ester was confirmed by FTIR spectroscopy (Figure S1). The content of the organic molecules in the synthesized nanoconjugate was calculated from the FTIR spectroscopy, elemental analysis (CHN) and thermogravimetric analysis data (Table S1, Figure S2). The size and morphology were studied using transmission electron microscopy and scanning electron microscopy analyses (Figure S3, S4). Dynamic light scattering (DLS) and zeta potential (*zP*) characterization were carried out using Malvern Zetasizer Nano ZS (Malvern Instruments, Malvern, UK) (Figure S5, Table S2).

The MDA-MB231 cells (human adenocarcinoma) were grown in 5% CO_2 at 37 °C in complete DMEM/F12 (HyClone, GE Healthcare Life Sciences, USA) media. The suspension of MNP-pHLIP in phosphate-buffered saline (PBS) was added to 10^5 MDA-MB231 cells seeded in a 24-well plate (1:10 vol./vol.) to a final concentration of 4-20 μg (Fe)/mL and incubated in media with pH 7.4 or 6.8 for 1 h. The iron concentration in cells was determined using colorimetric ferrozine-based assay [12].

Mouse and human peripheral blood mononuclear cells (PBMCs) were isolated using Ficoll density gradient centrifugation. Monocytes were isolated using Percoll (GE Healthcare Bio-Sciences AB, Uppsala, Sweden) double-density gradient centrifugation. Cell viability was measured using 7-aminoactinomycin D (Biolegend, USA) on a BD Accuri-C6 flow cytometer [11].

The animal study was approved by the Bioethics Review Committee of the Institute of Cytology and Genetics SB RAS (No. 38 on 18.07.2017). MDA-MB231 xenografts were transplanted into the right fat pad of female SCID (SHO-PrkdcscidHrhr) mice (n = 27) and permitted to grow for 6 to 8 weeks. The suspension of MNP-pHLIP or MNP-APS in PBS (100 μL) was administered to mice by the retro-orbital (venous sinus) route in a dose of 1 mg (Fe) per kg. The tumor-bearing mice that had been administered PBS were used as control. The mice were scanned both before and again 40 h after nanoparticle administration, using MRI on a horizontal tomographic scanner with magnetic field intensity of 11.7 T (Bruker, Biospec 117/16 USR, Germany).

After MRI scanning, the mice were sacrificed by cervical dislocation. Blood, liver, spleen, kidney, lung, thymus, left and right inguinal lymph nodes and tumor samples were collected. The concentration of the Fe ions in the tissue samples digested by nitric acid was measured using inductively coupled plasma atomic emission spectroscopy (ICP-AES) (iCAP 6300 Duo, Thermo Scientific).

Samples of the tumors varying in volume, extracted from randomly chosen mice in the control (n = 3), MNP-APS (n = 3) and MNP-pHLIP-injected (n = 4) groups were taken for TEM, histological examination and immunohistochemical analysis. The samples for TEM were prepared according to the procedure reported previously [13].

Statistical analysis was performed using GraphPad Prism (GraphPad Software).

More experimental details are given in Supplementary materials (Data in brief).

Results

Analysis of MNP-pHLIP in vitro

The ability of the nanoconjugate MNP-pHLIP to bind to MDA-MB231 cells in a pH-dependent manner was evidenced in *in vitro* experiments. The MDA-MB231 cells demonstrated an increase in MNP-pHLIP uptake at pH 6.8 in comparison with neutral pH (7.4) at concentration of nanomaterial above 10 mg/L (Figure 1).

Flow cytometry analysis of cell viability using 7-AAD showed that MNP-pHLIP caused no cytotoxic effects on MDA-MB231 cells after 48 h of incubation (Figure 1, *C*). Similarly, the amount of necrotic mouse PBMCs after 2 h of incubation with MNP-pHLIP (20 mg[Fe]/L) was equal to 7.4 ± 2.1%, and did not differ from the control (incubated with PBS) value (8.7 ± 1.7%, p = 0.29). Likewise, incubation of human and mouse monocytes with MNP-pHLIP (20 mg/L) for 24 h did not increase cell death (Figure S6).

Accumulation of nanoparticles in MDA-MB231 tumor

For the investigation of the influence of pHLIP-modification on the accumulation of nanoparticles in the tumors, parent unconjugated MNP-APS nanoparticles were used in the experiment. At 40 h after the administration of MNP-APS, we observed the reduction of T2-weighted signal from the tumors (Figure 2, *A*). The ICP-AES analysis revealed that the concentration of Fe in the tumor samples isolated 40 h after MNP-APS injection increased to 70 ± 30 μg/g (*vs* 45 ± 5 μg/g in the control group of PBS injected mice). In the meantime, in the group of mice that had been administered MNP-pHLIP the reduction of T2-weighted signal from the tumors was observed only in tumors with weight above 0.08 and below 0.4 g (medium-sized tumor) (Figure 2, *B*). Correspondingly, after MNP-pHLIP injection, according to ICP-AES data, the Fe concentration increased only in tumors with weight from 0.08 to 0.4 g and was equal to 76 ± 35 μg/g (Figure 2, *C*). Linear regression analysis showed the correlation of T2-weighted signal reduction with Fe concentration in tumors, determined according to ICP-AES (Figure S7).

The histological examination of the medium tumor (0.10 cm^3) extracted from one of the mice 40 h after MNP-pHLIP injection revealed Perl's positive cancer cells (Figure 3). Iron congestions were observed predominantly in the large metaplastic cells on the tumor periphery as well as in the extracellular matrix. According to Van Gieson's staining, we did not observe any difference in thickness or density of collagen in stroma among tumor samples of various volumes. Immunohistochemical analysis with CD31 antibodies showed that small capillary-like vessels are uniformly distributed in the small tumor (0.05 cm^3), whereas they are concentrated in the periphery of the medium tumor. The accumulation of MNP-pHLIP in the medium tumor was observed in a densely vascularized region.

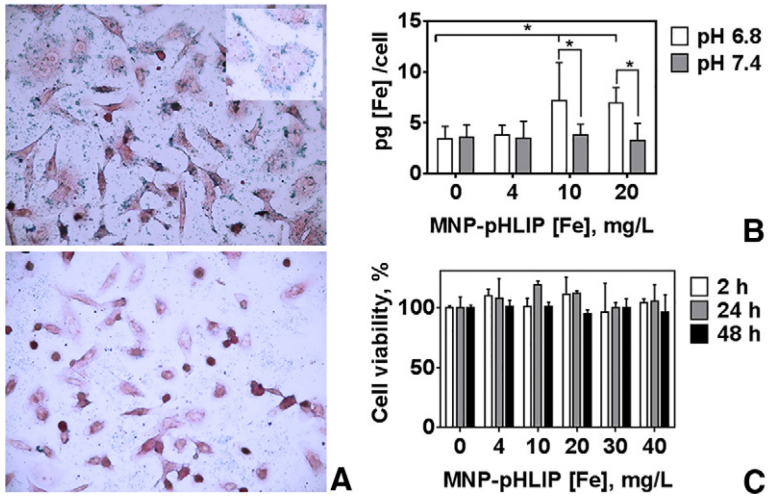

Figure 1. Interaction of MNP-pHLIP nanoconjugate with MDA-MB231 cells *in vitro*. (**A**) Prussian blue staining of MDA-MB231 cells incubated for 1 h with MNP-pHLIP (20 mg/L) at pH 6.8 (top) and pH 7.4 (bottom) shown at a ×400 magnification. **(B)** *In vitro* cellular uptake of MNP-pHLIP by MDA-MB231 cells at pH 6.8 (blank bar) and pH 7.4 (gray bar). (**C**) MDA-MB231 cells viability after incubation with MNP-pHLIP according to 7-AAD flow cytometry analysis. Data are shown as the mean ± SD. **P* < 0.05 *vs* control.

In the 0.5 cm^3 tumor, vessels are distributed diffusely, and the necrotic zone is concentrated in the tumor center.

The penetration of MNP-pHLIP in tumor cells was confirmed by TEM. The Fe_3O_4 clusters were found inside tumor cells in an autophagosome-like organelle (Figure 4, *A*, *B*) and in large vacuoles (Figure 4, *C-F*).

Interestingly, unlike control samples, tumors from mice treated with nanoparticles were infiltrated by eosinophils (Figure 5, Table S3). Eosinophils were found in three of four samples taken from mice treated with MNP-pHLIP, making up to 10% of cells per section. No eosinophils were observed in the untreated mice tumor samples or in the sample of MNP-pHLIP treated mice tumor with volume 0.5 cm^3.

MNP-pHLIP biodistribution and biocompatibility

ICP-AES measurements showed that the iron concentration in samples of the liver, spleen, kidney, lung and thymus resected from the mice 40 h after MNP-pHLIP administration did not differ from the control value (Table S4, Figure S8).

According to histological analysis 40 h after MNP-APS and MNP-pHLIP administration, no pathological changes were observed in the liver, spleen, kidney, lung, and thymus of the experimental animals (Figure S9). The serum parameters of the MNP-pHLIP-administered mice also did not differ from control (Table S5). A holistic interpretation of the data set indicates that MNP-pHLIP have no toxic effect for the duration of treatment.

Discussion

After retro-orbital administration MNP-pHLIP is able to accumulate in MDA-MB231 tumors and enter tumor cells. The initial insertion of the peptide in the cell membrane leads to further endocytosis *via* the formation of endosomes or lysosomes, and the subsequent fusion of late endosomes with autophagosomes results in the formation of amphisomes [14,15]. Nevertheless, the percentage of nanoparticles loaded cancer cells is relatively low. It is similar to that reported for 55 nm gold nanoparticle targeted by the ErbB2 receptor binding antibody [16].

The key findings of our study are: (a) dependence of MNP-pHLIP accumulation on tumor volume, with best results for medium-sized tumors (0.08-0.40 g), and (b) the strong association of MNP-pHLIP accumulation in tumors with dense blood vessel supply regions. Our results agree with Sykes's conclusions that the number of blood vessels available for nanoparticle entry is a key parameter determining the success of tumor targeting, and that nanoparticles with hydrodynamic diameter (D_h) > 100 nm demonstrate relatively short permeation distance in tumor from blood vessels [8]. However, Sykes's study showed that the increase in tumor size leads to the elevation in percentage of the gold nanoparticles accumulated in tumors, particularly for 100 nm nanoparticles, which demonstrate poor accumulation in tumors <0.5 cm^3 in volume. In our study the poor penetration of MNP-pHLIP (D_h = 142 nm) that was observed in the small tumors cannot be explained by nanoconjugate size, due to the fact that MNP-APS (D_h = 130 nm [11]) successfully accumulated in the small tumors with weight below 0.08 g. The conjugation of nanoparticles with pHLIP markedly changed the pattern of nanoparticle accumulation in comparison with the unconjugated one. One of the reasons for this is a change of surface charge after modification of nanoparticles by pHLIP from positive to negative [6] which leads to repulsion with negatively charged cell surface and abolishes nonspecific capture by cells [17].

Interestingly, PEGylated quantum dots/silica hybrid particles with D_h equal to 125 nm and *zP* equal to −9 mV did not penetrate in Mu89 human melanoma tumor (~0.01 cm^3) [18]. However, in the study of Jayapaul et al [19], the ultrasmall superparamagnetic iron oxide nanoparticles conjugated with flavin mononucleotide

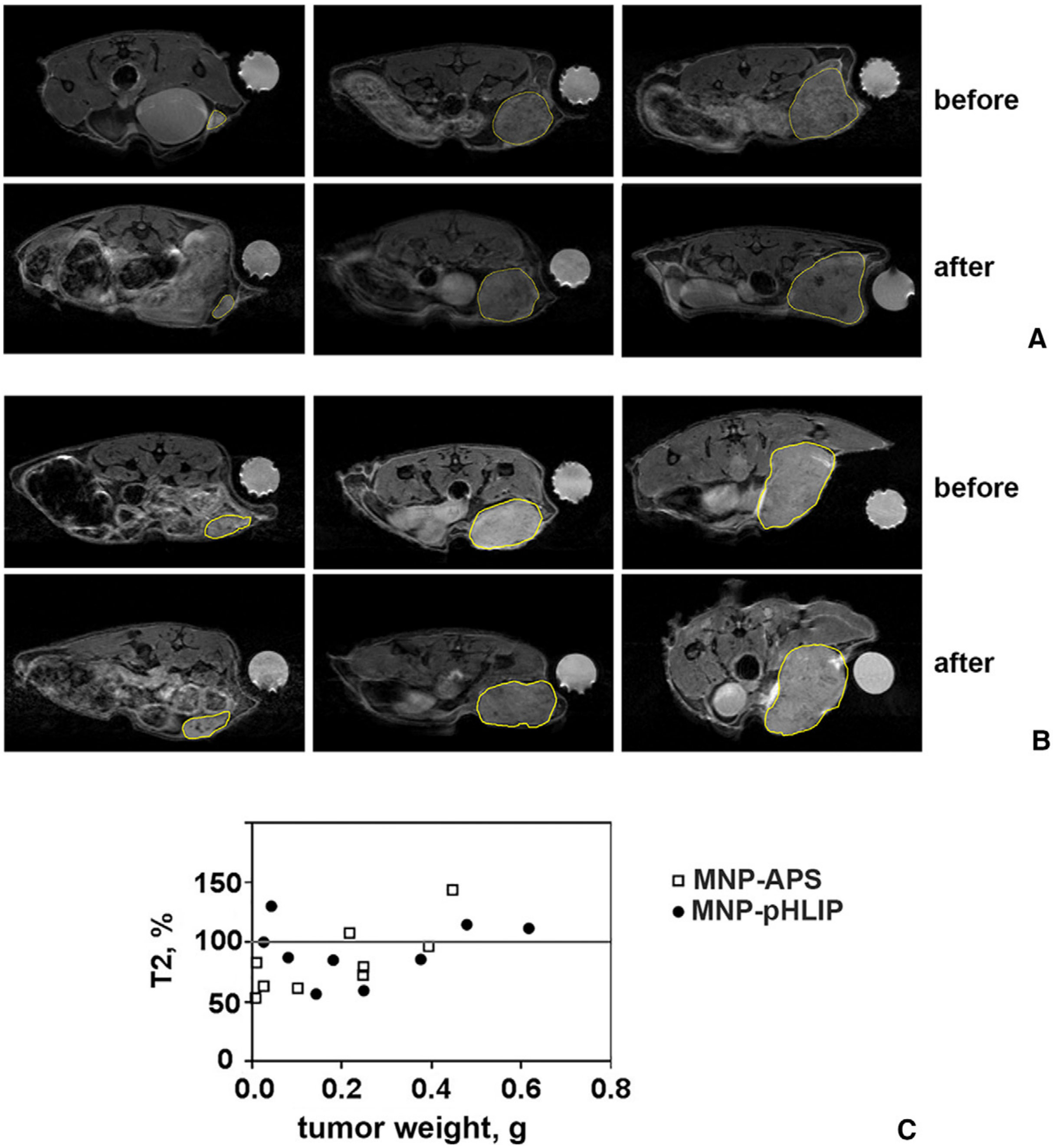

Figure 2. Magnetic resonance imaging of nanoparticle accumulation in MDA-MB231 breast tumor xenografts growing orthotopically in SCID mice. (**A**) T2-weighted MRI of the MDA-MB231 tumors before and 40 h after MNP-APS and (**B**) MNP-pHLIP administration recorded at 11.7 T (Bruker, Biospec 117/16 USR, Germany). (**C**) Percentage of the T2-weighted signal intensity of tumor recorded before and 40 h after MNP-APS and MNP-pHLIP administration.

(D_h = 107–134 nm, zP = −10 mV), successfully accumulated in LnCap tumor xenografts with volume 0.033 cm^3.

The discrepancy in the efficiency of MNP-pHLIP accumulation in MDA-MB231 *vs* gold nanoparticles accumulation in MDA-MB435 tumors with volume above 0.5 cm^3 can be attributed to the differences in the observed vessel distribution: uniformly in MDA-MB231 *versus* concentrated on the periphery and around necrotic zone in MDA-MB435 [8]. From this perspective, our results can be explained in terms of a constant remodeling of blood vessel architecture during tumor progression. Tumor vascularization starts 3 days after transplantation by sprouting new capillaries from the vessels in the surrounding host tissue [20]. During tumor progression, the diameter of vessels and their leakiness are increased [21], encouraging MNP-pHLIP tumor penetration. However, with the increase in tumor size, the vessels become more tortuous and, in patches, occluded, especially in the necrotic zone in the center of the tumor, thus hampering perfusion [20]. We should also emphasize that, according to data for mammary adenocarcinoma 72j transplanted in mice [21], vascular density and vessel surface area plateaued

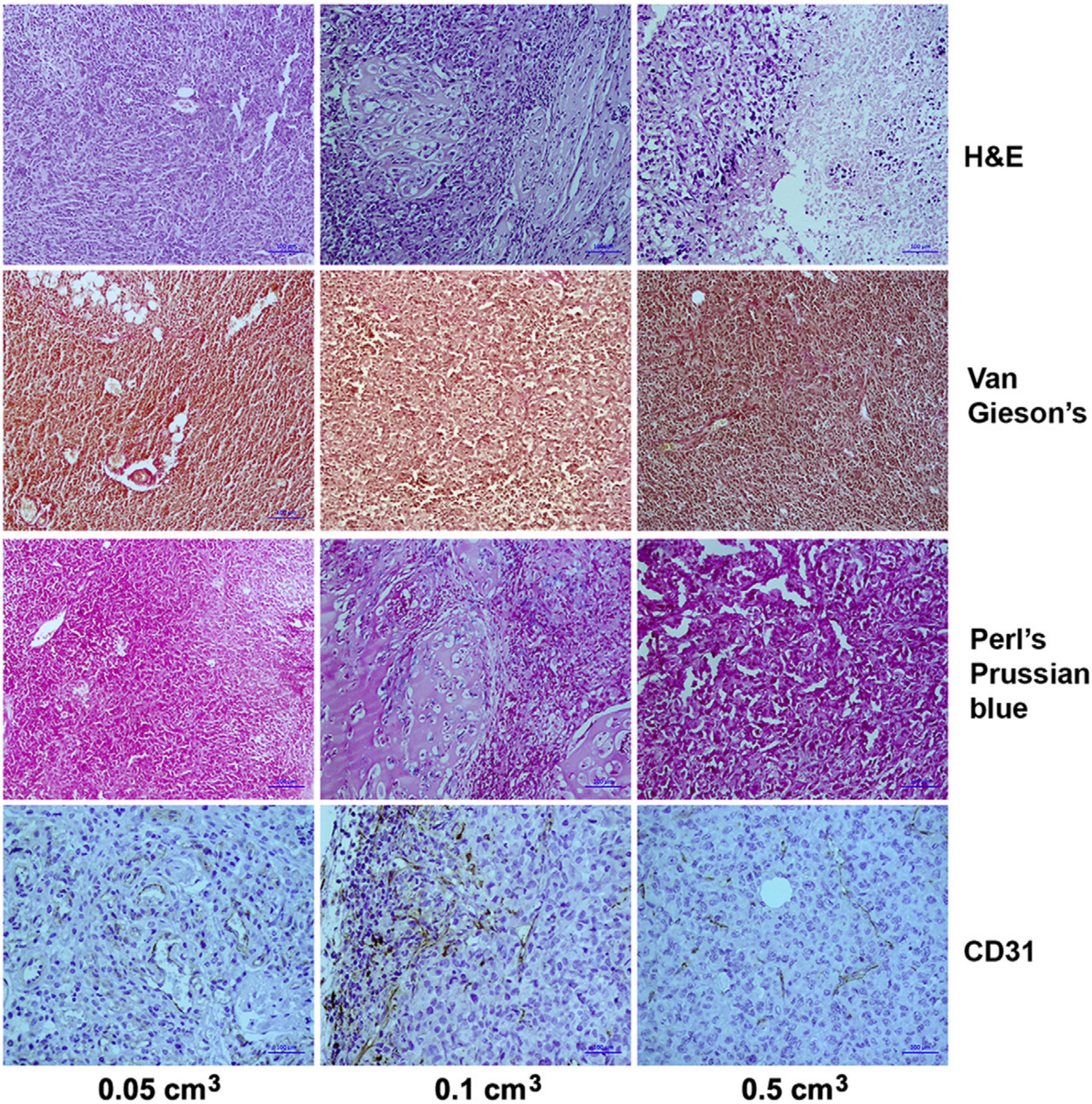

Figure 3. Analysis of MNP-pHLIP accumulation in MDA-MB231 breast tumor xenografts of small (0.05 cm^3), medium (0.1 cm^3) and large (0.5 cm^3) volume, growing orthotopically in SCID mice. Histological and immunohistochemical slides of the MDA-MB231 tumors extracted from mice 40 h after MNP-pHLIP administration. Perl's Prussian blue (for iron congestion), Van Gieson's (for collagen fibers) and CD-31 antibody followed by detection with EnVision FLEX/HRP (for vessel wall staining) were implemented.

after tumor reached volume ~0.5 g. In comparison, for MDA-MB435 melanoma cell line induced xenografts vascular density hits steady-state when tumor reached volume above 1.0 cm^3 [8]. Thus, the impact of the peculiarities of the used experimental cancer models should be taken into account [22,23]. Importantly the difference in vascularization between rapid and slow growing tumors [24] can be another reason for the aforementioned contradictions with the results of the studies. The successful targeting of 0.1 cm^3 MDA-MB231 tumors with intravenously administered pHLIP-microtubule inhibitor monomethylauristatin E conjugate has been shown by Burns et al [25].

Nanoparticle distribution in tumor is another highly relevant issue. According to Daniels's results, PEG-coated gold particles conjugated with pHLIP (D_h = 40–50 nm) were distributed almost homogeneously within JC mouse mammary gland adenocarcinoma ranging from 0.1 to 0.4 g 1 h after intratumoral injection, and the highest accumulation of gold was observed in the smallest tumors (~85 mg) [26]. In contrast to these results, unconjugated PEG-coated gold nanoparticles as well as gold nanoparticles coated with PEG and conjugated with anti-Her2 antibody accumulated predominantly in the tumor peripheries after intravenous injection in nude mice bearing BT-474 or

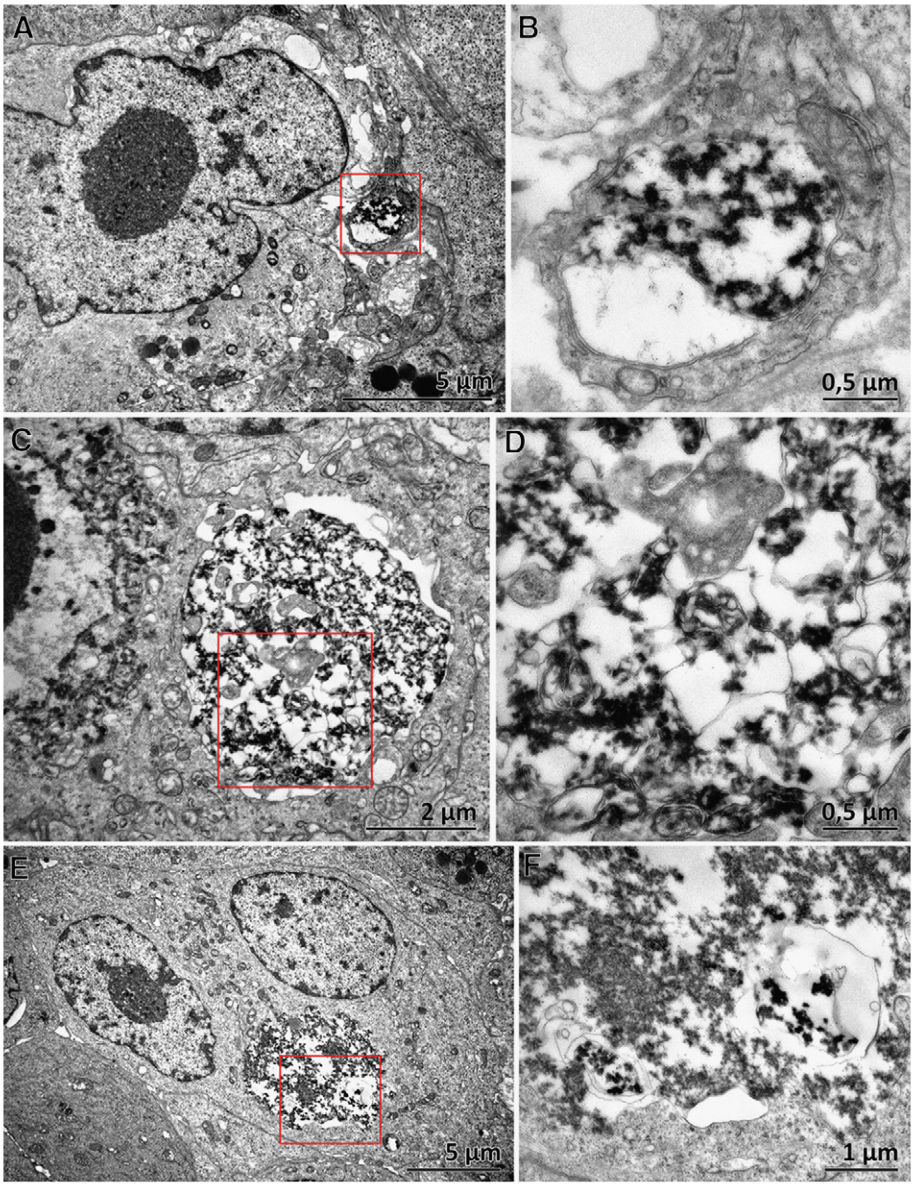

Figure 4. TEM images of iron oxide nanoparticles inside cells of MDA-MB231 xenografts treated with MNP-pHLIP. (**A**) A tumor cell containing a vesicle (most likely, amphisome) with the nanoparticle clusters. (**B**) Region magnified from red square on **A**, showing the vesicle. (**C-F**) Tumor cells with Fe_3O_4-containing vacuoles. (**D**) Region magnified from red square on **C**, showing the part of the vacuole with the nanoparticles. (**F**) Region magnified from red square on **E**.

MCF7 human breast tumors (60 mm^3) [27]. We consider that the route of administration, rather than the type of biomolecules, is the predominant contributory factor in nanoparticle distribution in tumors; and the above-mentioned results only strengthen the notion of the pivotal role of vessel distribution in nanoparticle delivery.

Another rationale is the direct correlation between tumor pH and tumor volume [28]; thus, the lack of pHLIP-mediated nanoparticle accumulation in the large tumors can be connected with an increase in tumor extracellular pH due to the growing influence of necrosis.

One interesting observation in our study was the abundance of eosinophils in tumors after nanoparticle injection. As shown by TEM, the treatment of mice with nanoparticles can summon eosinophils to the tumor. This state, Tumor-Associated Tissue Eosinophilia (TATE), is often associated with an improved prognosis for some types of cancers, including breast cancer [29,30]. The treatment with MNPs may itself have a protective effect by inducing TATE. This claim requires further research for support.

The Fe_3O_4 MNPs conjugated with pHLIP can target cancer cells of MDA-MB231 orthotopically induced tumors in SCID mice, but accumulation depends on tumor volume. Therefore, the cancer models used in a study, including tumor type and growth characteristics, may have the decisive role in the experiment's results. To ensure the success of nanomedicines in a clinical setting, the limitations of certain nanosystems must be established.

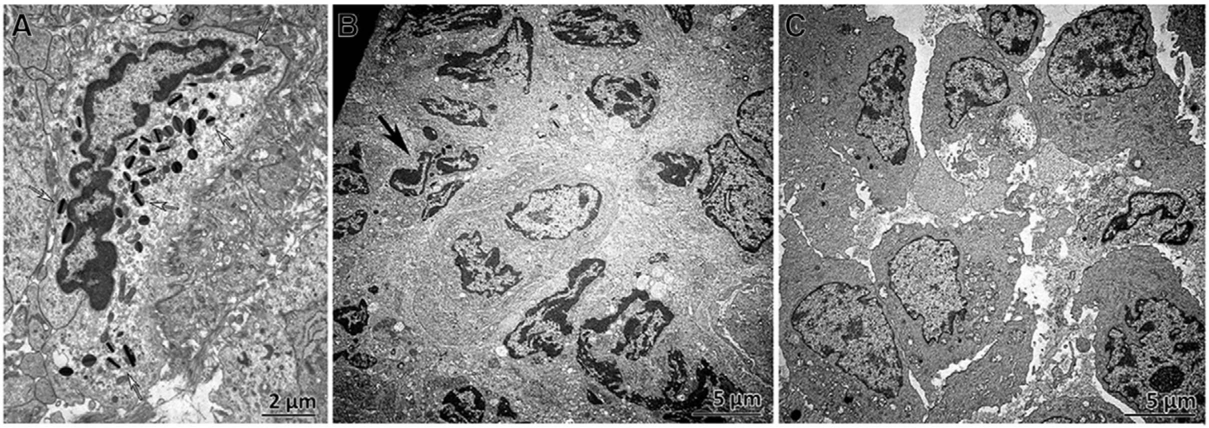

Figure 5. TEM images of mouse breast adenocarcinoma MDA-MB231 ultrathin sections with and without eosinophils. (**A**) A close-up image of an eosinophil infiltrating the tumor of a mouse treated with MNP-pHLIP. The specific granules (white arrows) are visible in its cytoplasm. (**B**) A fragment of the tumor section of an MNP-pHLIP-treated mouse with an eosinophil (black arrow). (**C**) A fragment of the tumor section of an untreated mouse (control) showing the absence of eosinophils.

Acknowledgments

The ICP-AES measurements was carried out using the core facilities of TPU's “Physical and chemical methods of analysis” (project VIU-RSCBS-142/2019).

The research in part of nanoparticle characterization was carried out within the framework of the state assignment theme (AAAA-A19-119011790130-3) at the Joint-Use Center for Spectroscopy and Analysis of Organic Compounds, Postovsky Institute of Organic Synthesis UB RAS.

The experiments with animals and MRI were carried out at the Center for Genetic Resources of Laboratory Animals at the Institute of Cytology and Genetics SB RAS, supported by the Ministry of Education and Science of Russia (Unique identifier of the project RFMEFI62117X0015).

TEM analysis was carried out at the Multiple-access Center for Microscopy of Biological Subjects, Institute of Cytology and Genetics SB RAS.

Appendix A. Supplementary data

Supplementary data to this article can be found online at https://doi.org/10.1016/j.nano.2019.102086.

References

1. Ellsworth RE, Blackburn HL, Shriver CD, Soon-Shiong P, Ellsworth DL. Molecular heterogeneity in breast cancer: state of the science and implications for patient care. *Semin Cell Dev Biol* 2017;**64**:65-72.
2. Juweid M, Neumann R, Paik C, Perez-Bacete MJ, Sato J, van Osdol W, et al. Micropharmacology of monoclonal antibodies in solid tumors: direct experimental evidence for a binding site barrier. *Cancer Res* 1992;**52**:5144-53.
3. Bae YH, Lee ES, Gao ZG. Recent progress in tumor pH targeting nanotechnology. *J Control Release* 2008;**132**:164-70.
4. Tian L, Bae YH. Cancer nanomedicines targeting tumor extracellular pH. *Colloids Surf B Biointerfaces* 2012;**99**:116-26.
5. Tapmeier TT, Moshnikova A, Beech J, Allen D, Kinchesh P, Smart S, et al. The pH low insertion peptide pHLIP variant 3 as a novel marker of acidic malignant lesions. *Proc Natl Acad Sci U S A* 2015;**112**:9710-5.
6. Demin AM, Pershina AG, Nevskaya KV, Efimova LV, Shchegoleva NN, Uimin MA, et al. pHLIP-modified magnetic nanoparticles for targeting acidic diseased tissue. *RSC Adv* 2016;**6**:60196-9.
7. Lammers T, Kiessling F, Hennink WE, Storm G. Drug targeting to tumors: principles, pitfalls and (pre-) clinical progress. *J Control Release* 2012;**161**:175-87.
8. Sykes EA, Dai Q, Sarsons CD, Chen J, Rocheleau JV, Hwang DM, et al. Tailoring nanoparticle designs to target cancer based on tumor pathophysiology. *Proc Natl Acad Sci U S A* 2016;**113**(9):E1142-51.
9. Loi M, Di Paolo D, Becherini P, Zorzoli A, Perri P, Carosio R, et al. The use of the orthotopic model to validate antivascular therapies for cancer. *Int J Dev Biol* 2011;**55**:547-55.
10. Demin AM, Pershina AG, Minin AS, Mekhaev AV, Ivanov VV, Lezhava SP, et al. PMIDA-modified Fe_3O_4 magnetic nanoparticles: synthesis and application for liver MRI. *Langmuir* 2018;**34**:3449-58.
11. Demin AM, Pershina AG, Ivanov VV, Nevskaya KV, Shevelev OB, Minin AS, et al. 3-Aminopropylsilane-modified iron oxide nanoparticles for contrast-enhanced magnetic resonance imaging of liver lesions induced by Opisthorchis felineus. *Int J Nanomedicine* 2016;**11**:4451-63.
12. Riemer J, Hoepken HH, Czerwinska H, Robinson SR, Dringen R. Colorimetric ferrozine-based assay for the quantitation of iron in cultured cells. *Anal Biochem* 2004;**331**:370-5.
13. Zakharova IS, Zhiven' MK, Saaya SB, Shevchenko AI, Smirnova AM, Strunov A, et al. Endothelial and smooth muscle cells derived from human cardiac explants demonstrate angiogenic potential and suitable for design of cell-containing vascular grafts. *J Transl Med* 2017;**15**:54.
14. Berg TO, Fengsrud M, Stromhaug PE, Berg T, Seglen PO. Isolation and characterization of rat liver amphisomes. *Evidence for fusion of autophagosomes with both early and late endosomes J Biol Chem* 1998;**273**:21883-92.
15. Fader CM, Sánchez D, Furlán M, Colombo MI. Induction of autophagy promotes fusion of multivesicular bodies with autophagic vacuoles in k562 cells. Traffic 2008:230–50.
16. Dai Q, Wilhelm S, Ding D, Syed AM, Sindhwani S, Zhang Y, et al. Quantifying the ligand-coated nanoparticle delivery to cancer cells in solid tumours. *ACS Nano* 2018;**12**:8423-35.
17. Chen B, Le W, Wang Y, Li Z, Wang D, Ren L, et al. Targeting negative surface charges of cancer cells by multifunctional nanoprobes. *Theranostics* 2016;**6**:1887-98.
18. Popović Z, Liu W, Chauhan VP, Lee J, Wong C, Greytak AB, et al. A nanoparticle size series for in vivo fluorescence imaging. *Angew Chem Int Ed Engl* 2010;**49**:8649-52.

19. Jayapaul J, Arns S, Bunker M, Weiler M, Rutherford S, Comba P, et al. In vivo evaluation of riboflavin receptor targeted fluorescent USPIO in mice with prostate cancer xenografts. *Nano Res* 2016;**9**:1319-33.
20. Forster JC, Harriss-Phillips WM, Douglass MJ, B E. A review of the development of tumor vasculature and its effects on the tumor microenvironment. *Hypoxia (Auckl)* 2017;**5**:21-32.
21. Vogel AW. Intratumoral vascular changes with increased size of a mammary adenocarcinoma: new method and results. *J Natl Cancer Inst* 1965;**34**(5):571-8.
22. Lode J, Fichtner I, Kreuter J, Berndt A, Diederichs JE, Reszka R. Influence of surface-modifying surfactants on the pharmacokinetic behavior of 14C-poly (methylmethacrylate) nanoparticles in experimental tumor models. *Pharm Res* 2001;**18**:1613-9.
23. Yokoi K, Kojic M, Milosevic M, Tanei T, Ferrari M, Ziemys A. Capillary-wall collagen as a biophysical marker of nanotherapeutic permeability into the tumor microenvironment. *Cancer Res* 2014;**74**:4239-46.
24. Lammers T, Peschke P, Kühnlein R, Subr V, Ulbrich K, Debus J, et al. Effect of radiotherapy and hyperthermia on the tumor accumulation of HPMA copolymer-based drug delivery systems. *J Control Release* 2007;**117**:333-41.
25. Burns KE, Robinson MK, Thévenin D. Inhibition of cancer cell proliferation and breast tumor targeting of pHLIP-monomethyl auristatin E conjugates. *Mol Pharm* 2015;**12**:1250-8.
26. Daniels JL, Crawford TM, Andreev OA, Reshetnyak YK. Synthesis and characterization of pHLIP® coated gold nanoparticles. *Biochem Biophys Rep* 2017;**10**:62-9.
27. Hainfeld JF, O'Connor MJ, Dilmanian FA, Slatkin DN, Adams DJ, Smilowitz HM. Micro-CT enables microlocalisation and quantification of Her2-targeted gold nanoparticles within tumour regions. *Br J Radiol* 2011;**84**(1002):526-33.
28. Engin K, Leepert DB, Cater JR, Thistlethwaite AJ, Tupchong L, NcFarlane JD. Extracellular pH distribution in human tumours. *Int J Hyperthermia* 1995;**11**:211-6.
29. Davis BP, Rothenberg ME. Eosinophils and cancer. *Cancer Immunol Res* 2014;**2**:1-8.
30. Sakkal S, Miller S, Apostolopoulos V, Nurgali K. Eosinophils in cancer: favourable or unfavourable? *Curr Med Chem* 2016;**23**:650-66.